Journal of Catalysis 283 (2011) 178–191

Contents lists available at SciVerse ScienceDirect

Journal of Catalysis

journal homepage: www.elsevier.com/locate/jcat

Microkinetic modeling of the fast selective catalytic reduction of nitrogen oxide with ammonia on H-ZSM5 based on first principles

Till C. Brüggemann [a,*], Dionisios G. Vlachos [b], Frerich J. Keil [a]

[a] Department of Chemical Engineering, Hamburg University of Technology, D-21073 Hamburg, Germany
[b] Department of Chemical Engineering, University of Delaware, Newark, DE 19716, USA

ARTICLE INFO

Article history:
Received 25 March 2011
Revised 28 June 2011
Accepted 20 August 2011
Available online 23 September 2011

Keywords:
Fast SCR
NO_2-SCR
ZSM5
Microkinetic modeling
Ammonia adsorption
Ammonium
Ammonia oxidation
Nitrosyl
Nitrosamine
Nitramide

ABSTRACT

The reaction mechanism of the fast selective catalytic reduction (SCR) of NO_x has been investigated by means of a microkinetic model based on DFT calculations. First, potential additional reaction mechanisms are presented that include the intermediate formation of $Z^-[NO_x]^+$ ($x = 1, 2$) from the decomposition of N_2O_y ($y = 3, 4$) on a Brønsted acid. The formed NO_x^+ reacts with ammonia to nirosamine or nitramide. The DFT results are applied in a microkinetic model together with prior studies of Brüggemann et al. The simulated conversion of NO_x is in agreement with experimental data over a wide range of temperature. The activity of the H-ZSM5 for the fast SCR is based on the reaction sequence via $Z^-[NO_x]^+$, the decomposition of nitrosamine and nitramide, and the reaction of nitrous and nitric acid with adsorbed ammonia at low temperatures. Ammonia blocks the active sites at low temperatures while thermodynamic limitations of the surface species N_2O_y restrict the conversion at high temperatures. Heat of formations and reaction rate constants were adjusted within the accuracy of the applied method for important elementary steps to cope with experimental data.

© 2011 Elsevier Inc. All rights reserved.

1. Introduction

Nitrogen oxides (NO, NO_2), which are mainly produced in the combustion of fossil fuels, are significant air pollutants, and stringent emission standards have been legislated to regulate exhaust gases [1,2]. The selective catalytic reduction (SCR) with ammonia or hydrocarbons has proven to be an effective technology for the abatement of NO_x and has been in the focus of researchers for the last two decades [3–5]. In particular, metal-exchanged zeolites like the Fe/H-ZSM5 were found to exhibit a high activity for this reaction [6]. The boosting effect of NO_2 upon addition to the reactant gas [7–11] or via a pre-oxidation step within the SCR converter was a crucial finding in the ammonia SCR. The highest conversion is obtained with a NO_2/NO_x ratio of 50% which is known by now as the "fast" SCR according to the stoichiometric equation

$$2NH_3 + NO + NO_2 \rightarrow 2N_2 + 3H_2O \quad (1)$$

Dosing a ratio above the 50% results in a slightly reduced activity and an increased selectivity to unwanted N_2O. The "NO_2-SCR" [12] marks the outer boundary with only NO_2 in the reactant gas. Furthermore, metal-exchanged zeolites were also found to exhibit a significant activity for the selective oxidation of ammonia (SCO) [13–20], which has to be considered a side reaction of the SCR. However, based on the usual preparation from ion exchange to a parent H-form zeolite, the final catalyst usually exhibits two different active sites, the exchanged metal and the Brønsted acid. Brandenberger et al. [6] even stated an amount of at least 30% of the latter one. While the standard SCR is known to be much slower on the H-form zeolites than on the iron-exchanged catalyst, a significantly high activity was observed for the fast [7,10,11,21,22] and the NO_2-SCR [23]. Also for the SCO, a significant activity was observed on the Brønsted acid sites [14,15,24]. This raised the question regarding the influence of the Brønsted acids in iron-exchanged zeolites. Long and Yang [11] concluded that the iron in Fe/H-ZSM5 is only responsible for the oxidation of NO to NO_2 while the fast SCR is catalyzed by the Brønsted acids only. In contrast, Devadas et al. [7] and Grünert et al. [10] found a higher activity of the iron containing zeolite for the fast SCR, too. Nevertheless, both groups attributed an at least promoting effect of the Brønsted acid to the activity of the catalyst [25,26]. This is, according to Akah et al. [15], also true for the SCO. Thus, in order to understand the mechanisms of the reactive H/N/O system in iron-exchanged zeolites, analysis of important elementary steps on both active sites, the iron and the Brønsted acid, is crucial. Recently, we [27–29] have established a reaction network for the H-form zeolite using density

* Corresponding author.
E-mail address: till.brueggemann@tu-harburg.de (T.C. Brüggemann).

0021-9517/$ - see front matter © 2011 Elsevier Inc. All rights reserved.
doi:10.1016/j.jcat.2011.08.009

functional theory (DFT) that qualitatively accounts for most experimentally observed phenomena (see Fig. 24 in Ref. [29]) for both the SCR and the SCO. In general, we concluded that in the mechanism of the fast and NO_2-SCR, the intermediate N_2O_y ($y = 3, 4$) forms, which, after the reaction with ammonia, leads to nitrous and nitric acid and finally to nitrosamine and nitramide. For the SCO, we identified nitroxyl and hydroxylamine as key intermediates. However, in these investigations, we only considered a direct reaction of the N_2O_x with on Brønsted acids adsorbed ammonia as the initial step of the SCR. Richter et al. [30] pointed out that the dehydration of intermediately formed nitrous acid could form the nitrosyl cation NO^+, which is known from organic chemistry to be capable of attacking amines under the formation of N-nitroso amines. In the simplest case, the reaction of ammonia with NO^+ forms nitrosamine (NH_2NO), which easily decomposes on H-ZSM5 into nitrogen and water. In fact, the nitrosyl cations in H-form zeolites are well known from several studies on the adsorption of NO_x in these catalysts [31–34] and correspond to an IR band at 2133 cm^{-1}. Lavalley and coworkers [31] suggested the formation of NO^+ from the decomposition of N_2O_3 adsorbed on a Brønsted acid by forming nitrous acid. The latter dehydrates then on a second acid site in analogy to the mechanism proposed by Richter et al. [30] and Lavalley and coworkers [31]. A combination of these two suggestions leads to a reasonable reaction pathway for the fast SCR according to

$$Z\_H^+ + NO + NO_2 \leftrightarrow Z\_H^+ - N_2O_3 \leftrightarrow Z\_NO^+ + HONO \quad (2)$$

$$Z\_H^+ + HONO \leftrightarrow Z\_NO^+ + H_2O \quad (3)$$

$$Z\_NO^+ + NH_3 \leftrightarrow Z\_H^+ + NH_2NO \quad (4)$$

In analogy, one can suggest the formation of a NO_2^+ species balancing the charge of the zeolite framework as was done by Busca and coworkers [21]. The formation of this species could then either be explained by the decomposition of nitric acid in analogy to reaction (3) or by the decomposition of adsorbed N_2O_4 forming nitrous acid in analogy to reaction (2).

$$Z\_H^+ + NO_2 + NO_2 \leftrightarrow Z\_H^+ - asN_2O_4 \leftrightarrow Z\_NO^+ + HNO_3 \quad (5)$$

$$Z\_H^+ + NO_2 + NO_2 \leftrightarrow Z\_H^+ - symN_2O_4 \leftrightarrow Z\_NO_2^+ + HONO \quad (6)$$

$$Z\_H^+ + HNO_3 \leftrightarrow Z\_NO_2^+ + H_2O \quad (7)$$

$$Z\_NO_2^+ + NH_3 \leftrightarrow Z\_H^+ + NH_2NO_2 \quad (8)$$

In analogy to reaction (4), the NO_2^+ species can then react with ammonia (reaction (8)) to nitramide (NH_2NO_2) that decomposes to nitrous oxide and water. Finally, an interchange of the two NO_x^+ species according to

$$Z\_NO_2^+ + NO \leftrightarrow Z\_NO^+ + NO_2 \quad (9)$$

is at hand. The sequence of reactions (2)–(8) is in agreement with the experimentally observed stoichiometry of the fast and the NO_2-SCR. Nevertheless, only a direct comparison of the theoretically derived mechanisms with experiments allows for a final conclusion of the accessible pathways. Microkinetic modeling has been applied extensively with success in order to provide insight into the mechanisms of several heterogeneous catalyzed reactions [35–40]. Results from first principles methods like DFT can be used to provide the required parameters for a kinetic model that then closes the gap between microscopic and macroscopic quantities. The goal of this work is to establish a microkinetic model based on our previous work [27–29] as well as to include the investigation of the potential formation of NO_x^+ species according to Eqs. (2)–(9). This implies two parts, first, the analysis of the proposed additional reaction mechanisms by using DFT and, second, the analysis of all elementary steps of the system in a reactor simulation. In comparison with experimental data, this analysis is supposed to provide significant insight into the governing elementary steps of the combined SCR and SCO system on H-ZSM5 and with that to allow for suggestions on interactions of intermediates in the ion-exchanged zeolites in further studies. This study is intended to present a basis to which the contribution of metal ions can be added and to build an understanding of the complex chemistry in the real catalyst, starting from the most reduced catalyst, the parent H-form. The impact of iron as metal ion is the subject of our present research.

2. Theory

As a representation of the active site for the analysis of reactions (2)–(9), a cluster of 5 T-sites (see Fig. S1, Supporting information) with the Si atoms, initially placed at their crystallographic positions [41] and saturated with hydrogen atoms, was used. The framework cluster was cut from the unit cell so that it surrounds the T12 site that was suggested to be the most probable position of the Al [42–46]. The terminal Si atoms were saturated with hydrogen atoms that were held fixed for all calculations on the catalyst. The Brønsted acid site is the hydrogen bonded to the bridging oxygen atom. In order to include, at least to a certain extent, the influence of the pore structure on the reactants and products, energy minimizations were executed for selected species of the complete reactive system on a 23 T-sites containing portion of the catalyst (Fig. 1). From Table S2 in the Supporting information, it can be obtained that the impact of the larger cluster on the electronic energy as compared to the five T-atoms containing cluster is only relevant if ammonia, water, or hydroxylamine is present.

All quantum chemical calculations on the catalyst were carried out with the TURBOMOLE suite of programs [47] by using gradient-corrected density functional theory (DFT). We used Becke's 3-parameter exchange functional [48] and the correlation functional of Lee et al. [49] (B3LYP) together with the triple-ζ basis set with polarization functions (TZVP) [50] for all atoms and a very fine numerical grid size (m5) [51]. Structure optimizations were

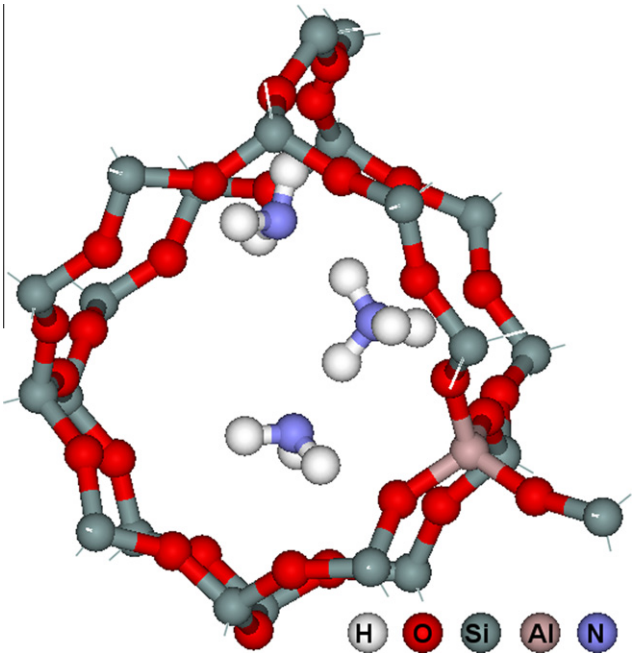

Fig. 1. T23 cluster model of the acid site in the intersection of a straight and a zigzag pore of H-ZSM5 with three co-adsorbed ammonia molecules. Dangling bonds are not shown.

performed in Cartesian coordinates with an energy convergence criterion of 10^{-7} Ha, and the maximum norm of the Cartesian gradient was converged to 10^{-4} Ha/bohr. The CBS-QB3 level was applied with Gaussian 03 [52] in order to obtain sufficiently accurate heats of formation for those gas-phase intermediates for which no reliable experimental data were available.

Transition states on one potential energy surface (PES) were localized using first the growing string-method [53] to obtain an approximate saddle point which was then refined by either the modified dimer method [54] or the PRFO method [55]. In cases of different spin states of reactants and products, a multiplier penalty function algorithm (see Heyden et al. [56] for details) was applied to find the minimum energy crossing point (MECP) structures on the seam of the two PESs.

For microkinetic modeling, CHEMKIN [57,58] was employed. The required thermodynamic parameters of the species and the kinetic parameters for the reactions were derived according to standard statistical thermodynamics [59,60] and transition state theory [61] on the basis of the DFT results. For the ad/desorption processes, the theory of absolute rate [61] was applied for the desorption, assuming the barrier to be equal to the zero-point energy (ZPE) corrected energy difference between the adsorbed and the desorbed state. This implies a barrierless adsorption for which the rate is obtained from the equilibrium constant and the rate of desorption. Such an approach, which relies on the idea of transition state theory, neglects any difference in entropy of the adsorbed state and an assumed transition state of desorption. This, however, can result in a significant underestimation by several orders of magnitude in the pre-exponential factor for loose transition states as outlined by Chorkendorff and Niemantsverdriet [62]. Assuming that transition states of desorption are rather loose in the case of physisorption, the corresponding rates of mechanistic relevant steps can be expected to require significant fine-tuning. Nevertheless, this approach is expected to yield reasonable first estimates for the model.

The harmonic approximation was applied, and contributions for the translational, rotational, vibrational, and electronic partition function were considered for all gas-phase species while for the zeolite cluster, only the vibrational and electronic contributions were included. Enthalpy, entropy, and the heat capacity were simultaneously fitted to the in CHEMKIN required seven-parameter polynomial for all species using the algorithm of Spitzer et al. [63]. In order to calculate rates for the crossing of PESs, adoptions to adiabatic TST can be used [64,65]. According to Harvey [65], the calculation of the thermal rate constant can be calculated, in good approximation, as the product of a mean probability of surface hopping and a hypothetical adiabatic rate constant resulting from a transition state with the same relative energy and properties of the MECP. While translational and rotational contributions are directly related to the structure of the MECP, the evaluation of the vibrational contribution to the partition function requires the calculation of an effective Hessian as outlined by Harvey et al. [66,67]. It can be written as

$$\mathbf{H}_{eff} = \pm\frac{|\mathbf{g}_1|}{|\mathbf{g}_1 - \mathbf{g}_2|}\cdot\mathbf{H}_2 \pm \frac{|\mathbf{g}_2|}{|\mathbf{g}_1 - \mathbf{g}_2|}\cdot\mathbf{H}_1 \tag{10}$$

with $\mathbf{H}_1$ and $\mathbf{H}_2$ representing the Hessian matrixes and $\mathbf{g}_1$ and $\mathbf{g}_2$ the gradients of the energy at the MECP on the PESs with spin state "1" and "2". It is derived from the Taylor expansion of a Lagrangian at the MECP as outlined by Koga and Morokuma [68], and the signs of the two fractions are dependent on the sign of the Lagrange multiplier. The derivation is shown in Appendix A. Finally, the translational and rotational degrees of freedom as well as the gradient difference ($\mathbf{g}_1$–$\mathbf{g}_2$) have to be projected out of the effective Hessian (see Page and McIver [69] for details). The surface thermally averaged hopping probability can be calculated from the Landau–Zener theory [70]. However, because the direct comparison of calculated and experimentally measured reaction rate constants for the decomposition of N_2O_3 and N_2O_4 in the gas-phase revealed that the theoretically derived pre-exponential factors of the Arrhenius equation are rather too low, even without the hopping probability, we set the latter in all cases equal to 1.

Furthermore, it is known that the accuracy of DFT in the calculation of relative energies as well as for reaction barriers is limited [71] (±5 kcal/mol), usually allowing only for a qualitative analysis of reaction pathways. According to Gokhale et al. [39], DFT can capture the essential aspects of the surface chemistry but fine-tuning usually needs to be done to obtain a reliable microkinetic model. Even though there are quantum chemistry techniques that can provide nearly quantitative results for intrinsic reaction steps, as recently shown by Hansen et al. [72], their application to reactive systems with large number of elementary steps is not feasible because of the high computational cost. To obtain reliable heats of formation of the surface species, the values were anchored to the gas-phase species thermochemistry. This was done by relating the heat of formation of the surface species to the corresponding heat of adsorption of a gas-phase species on the empty active site. For the latter, the heat of formation was set to $\mathbf{H}_f = 0$ (denoted as HZSM5 in the thermodynamic database S3). Because the heat of formation of the gas-phase species is, in the best case, experimentally measured or at least calculated with high level methods, inaccuracies in the surface reaction enthalpies, which are computed with the lower DFT level, can be corrected to a certain extent. Furthermore, it is known that the generalized gradient approximation (GGA) functionals in DFT do not include the long-range electron correlations responsible for van der Waals forces. Grimme [73] has calculated parameterizations for a DFT-D approach to include damped atom pair-wise dispersion corrections of the form C_6R^{-6} for several functionals. To correct the heats of adsorption, we have applied this scheme to all surface species using the results from the 23 T-site containing cluster as far as available and approximated values for the remaining species based on the comparison of the T5 vdW contributions. This was done by either assigning the same vdW values for similar structures, by adding a T23-T5 vdW difference or by adding a T5 contribution to a reference state for which a T23 contribution is available. The applied method is documented for all species in Table S1 in the Supporting information. This is a compromise between accuracy and computational costs for the calculations on the larger cluster. Finally, a common assumption for the adsorption is the complete loss of the rotational and translational degrees of freedom of the adsorbate being transferred into vibrational degrees. While this is reasonable for small molecules in chemisorption in the case of physisorption, it might lead to a significant underestimation of the entropy of adsorption. A potential technique to overcome this problem is the reassignment of restricted translational and rotational degrees of freedom in exchange of the corresponding vibrations. Dumesic et al. [39] proposed a restricted translation in terms of surface diffusion. Reyniers and coworkers [74] reassigned contributions of the rotation in a zeolite by including the principle moments of inertia representing the as free considered motion of the corresponding gas-phase species. For translation, a movement within a plane perpendicular to the active site was considered. The size of this plane was related to a certain extent to the pore diameter and to the size of the zeolite cages. We used the methodology of Reyniers and coworkers [74] to obtain an order of magnitude estimate for entropy corrections for species that are rather loosely adsorbed or co-adsorbed. This affects mainly N_xO_y species as well as HNO_z co-adsorbed to NO_x^+ (see Table S1, Supporting Information). The applied values are based on calculations for physisorbed NO_2 and

asymmetric N_2O_4 for which we obtained entropy corrections ΔS_{trans} = 3.8 cal/mol/K and ΔS_{trans} = 6.6 cal/mol/K for the 2D translation on a surface of A^0/N_A = 700 pm * 700 pm and ΔS_{rot} = 3.1 cal/mol/K and ΔS_{rot} = 5.6 cal/mol/K for a 1D rotation at 600 K. It should be noted that according to Cramer [60], the exchange of vibrational frequencies by restricted translations or rotations should also affect the contribution to the enthalpy. A low frequency that represents the harmonic oscillator approximation of a frustrated translation or rotation results into a contribution of RT, but the contribution of a free translation or rotation contributes only 0.5 RT per degree of freedom. Thus, at a temperature of 600 K, the exchange of four degrees of freedom leads to an underestimation of the heat of adsorption of ΔE = 2.4 kcal/mol. With that, also the assigned heat of formation of the corresponding surface species is affected. Though this value is not significant at first glance, it might have a great impact in the case that the overall reaction exhibits a high sensitivity on such an intermediate. Thus, this energy contribution can also be taken into account in the fine-tuning of a microkinetic model.

Despite the discussed potential corrections that can be applied to improve the model, the uncertainties of the electronic energy as calculated from DFT still remain and with that the rather qualitative nature of the values. Nevertheless, significant insight into the mechanisms of the reactive H/N/O system can be obtained from such an approach.

3. Results and discussion

To complete our previous investigations of the fast and the NO_2-SCR on the H-ZSM5 [27–29], we present here the additional reaction pathways according to Eqs. (2)–(9) by applying DFT. In the second part, we will then discuss the results obtained from the microkinetic modeling, involving also all the reactions of our previous theoretical investigations of the H/N/O system.

3.1. DFT Results for the fast and the NO_2-SCR

Starting with the fast SCR, the reaction cycle is shown in Fig. 2 with the numbers being the zero-point-corrected energies relative to the gas-phase and the empty catalyst. The energies are also shown in the corresponding diagram (Fig. 3), and the structures are presented in the Supporting information (Fig. S2). The mechanism starts with the weak adsorption of NO_2 on the Brønsted acid (ST1). The subsequent co-adsorption of NO reveals only a negligible interaction between the two molecules (ST2). However, only a small barrier of $E^{\ddagger}$ = 1.4 kcal/mol, associated with the crossing of the seam (S2) from the triplet to the singlet PES, needs to be overcome to form asymmetric (as) N_2O_3 (ST4). Alternatively, the slightly less stable cis-trans (ct) N_2O_3 (ST3) is formed by overcoming a barrier of $E^{\ddagger}$ = 4.5 kcal/mol (S1). Subsequently, the dimerized nitrogen oxide decomposes whereby the NO becomes a nitrosyl ion on the catalytic framework ($Z^-[NO]^+$) and the NO_2 takes up the hydrogen from the surface by forming nitrous acid (ST5). In the case of as-N_2O_3 as starting point, this process exhibits an activation energy of $E^{\ddagger}$ = 5.3 kcal/mol (TS1) while a barrier of $E^{\ddagger}$ = 0.1 kcal/mol (TS2) was calculated for the ct-N_2O_3. Though the initial formation of the asymmetric dimerized nitrogen oxide is preferred over the cis-trans configuration, the subsequent decomposition of the cis-trans species probably is faster because of the negligible small activation energy. Thus, both pathways can be expected to be accessible. As the next step, the nitrous acid desorbs from the catalyst leaving the $Z^-[NO]^+$ (ST6), which involves a heat of desorption of ΔE_{des} = 9.7 kcal/mol. Finally, ammonia adsorbs onto this species (ST8) with a heat of adsorption of ΔE_{ads} = 10.8 kcal/mol prior to the reactive formation of nitrosamine (ST10). The ammonia releases one proton to the catalyst by restoring the Brønsted acid, and the remaining amino radical takes up the NO^+ from the surface. The barrier of this step was determined to be $E^{\ddagger}$ = 2.9 kcal/mol, represented by TS4. The formed NH_2NO then decomposes on the Brønsted acid as described in Ref. [27].

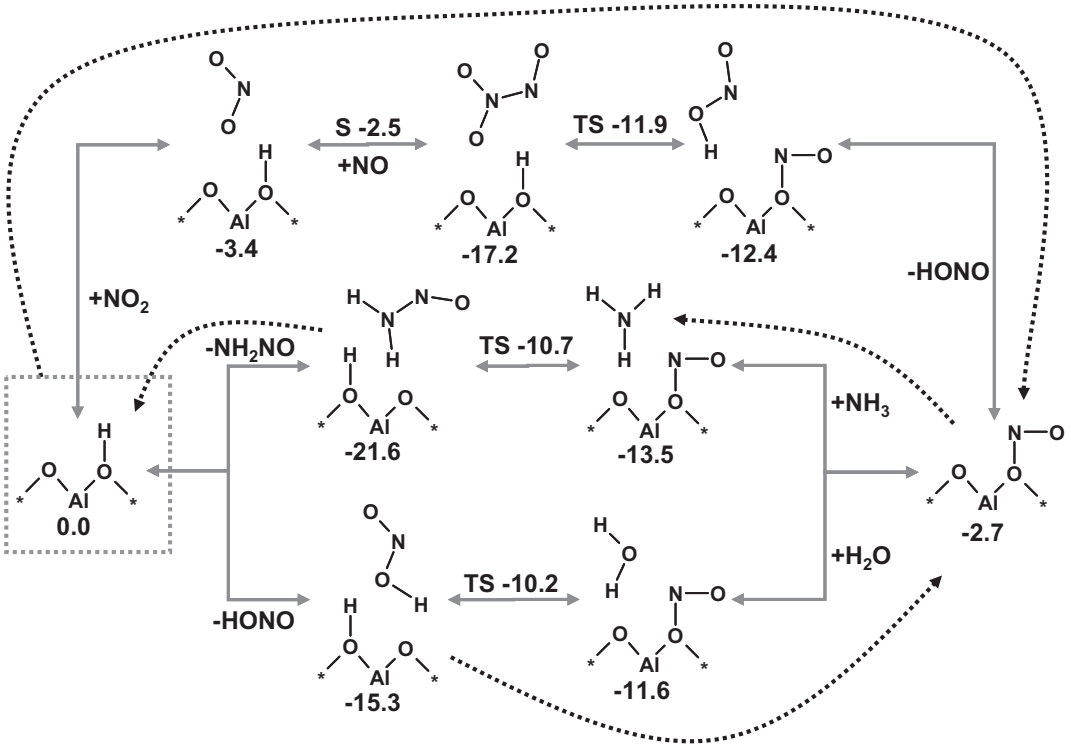

Fig. 2. Reactive cycle of the fast-SCR mechanism including transition states (TS) and a minimum energy crossing point (S). Numbers are zero-point-corrected energies relative to the gas-phase and the empty catalyst. Additional black dotted arrows outline the relevant pathway.

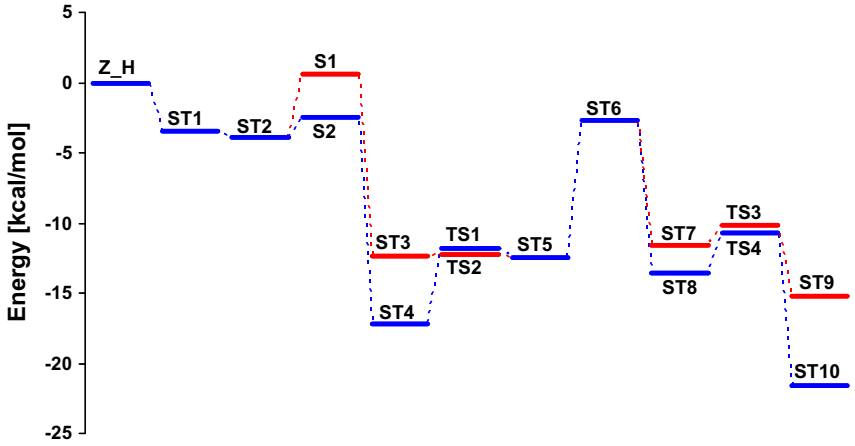

Fig. 3. Energy profile of the fast-SCR mechanism comparing two routes via asymmetric and cis-trans N_2O_3. Energies are zero-point-corrected.

Alternatively, water co-adsorbs onto the $Z^-[NO]^+$ intermediate (ST7) with a heat of adsorption ΔE_{ads} = 8.9 kcal/mol. A subsequent reaction, analogous to the mechanism with ammonia, leads to the formation of nitrous acid (ST9) by overcoming a barrier of $E^{\ddagger}$ = 1.4 kcal/mol (TS3). Though the latter step is exothermic and only exhibits a rather small barrier, within the framework of the SCR also the reverse reaction could be of significance in terms of a sink for the intermediate produced nitrous acid from the decomposition of N_2O_3.

In the case of the NO_2-SCR, the overview of the reaction cycle is shown in Fig. 4 and the corresponding energy diagram is displayed in Fig. 5. The structures of all species are shown in the Supporting

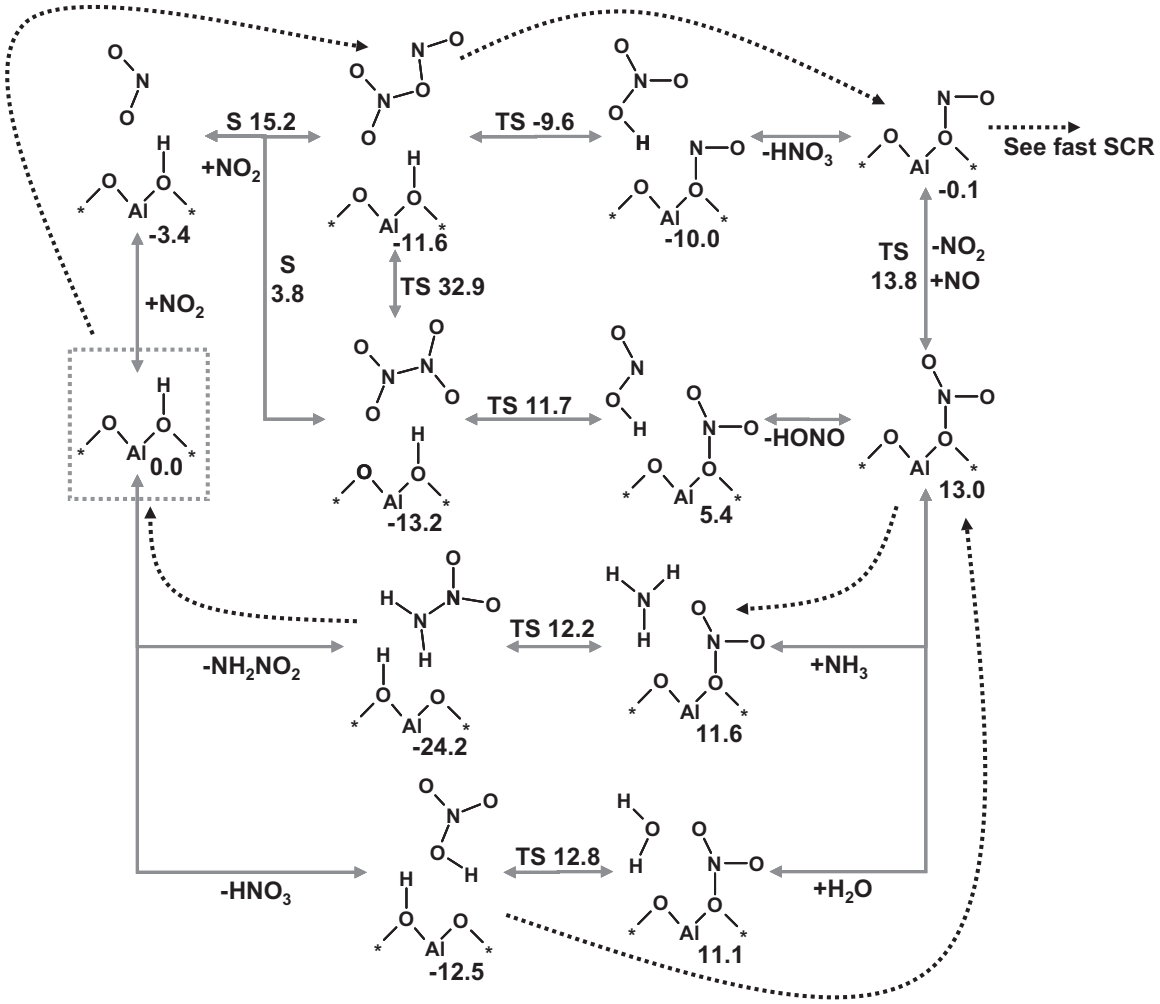

Fig. 4. Reactive cycle of the NO_2-SCR mechanism including transition states (TS) and minimum energy crossing points (S). Numbers are zero-point-corrected energies relative to the gas-phase and the empty catalyst. Additional black dotted arrows outline the relevant pathway.

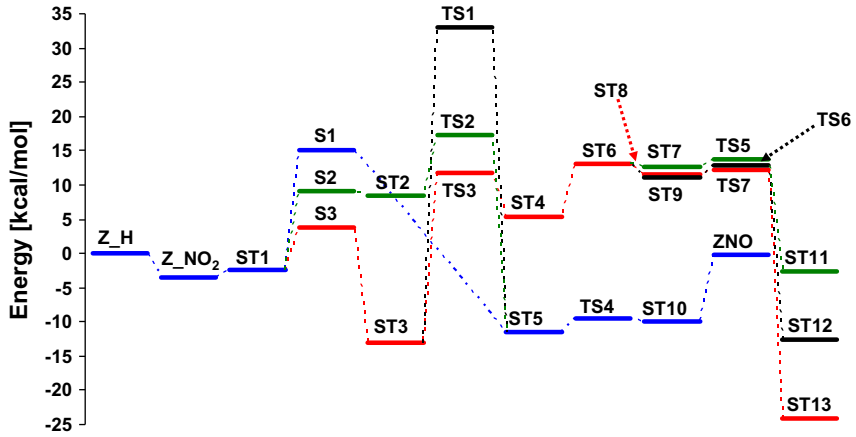

Fig. 5. Energy profile of the NO_2-SCR mechanism comparing three routes via symmetric, asymmetric, and cyclic-planar N_2O_4. Energies are zero-point-corrected.

information in Fig. S3. After the co-adsorption of two NO_2 (ST1), the formation of a dimerized N_2O_4 takes place by crossing the seam from the triplet to the singlet PES in analogy to the fast SCR. Here, three different structures are possible, a symmetric (sym) (ST3), an asymmetric (as) (ST5), or a cyclic-planar (cp) N_2O_4 (ST 2). The lowest barrier was calculated for the first case with a barrier of $E^{\ddagger}$ = 6.3 kcal/mol (S3), followed by the cyclic-planar isomer with $E^{\ddagger}$ = 11.6 kcal/mol (S2) and finally $E^{\ddagger}$ = 17.7 kcal/mol (S1) for the asymmetric case. However, the formation of the cyclic-planar isomer is less favorable than the asymmetric or symmetric N_2O_4 because of an endothermic reaction in contrast to an exothermic heat of reaction for the latter two cases. The cp-N_2O_4 can be transferred into the asymmetric isomer by overcoming a barrier of $E^{\ddagger}$ = 8.9 kcal/mol (TS2), but as can be seen from the energy diagram, no benefit can be deduced from this alternative route as compared to the direct formation of the as-N_2O_4. Also the symmetric isomer can be transformed into the asymmetric one, but because this process exhibits a rather high activation energy of $E^{\ddagger}$ = 46.1 kcal/mol (TS1), it can be excluded. Starting from the as-N_2O_4, the decomposition of the molecule results in the formation of nitric acid and an NO^+ to balance the negative charge of the zeolite framework (ST10). Here, the mechanism is in analogy with the $Z^-[NO]^+$ formation from the decomposition of N_2O_3, and the barrier, according to the transition state TS4, was calculated to be $E^{\ddagger}$ = 2.0 kcal/mol. Finally, the desorption of nitric acid, with a heat of desorption of ΔE_{des} = 9.9 kcal/mol, leaves the nitrosyl ion on the surface for the reaction with ammonia as described above. Similarly, the decomposition of sym-N_2O_4 leads to the formation of nitrous acid together with $Z^-[NO_2]^+$. This process exhibits a barrier of $E^{\ddagger}$ = 24.8 kcal/mol (TS3) and is endothermic by ΔE = 18.5 kcal/mol (ST4). The desorption of the nitrous acid requires then a heat of desorption of ΔE_{des} = 7.6 kcal/mol. In analogy to the reaction with $Z^-[NO]^+$, the $Z^-[NO_2]^+$ (ST6) can also react with both ammonia and water. In the first case, ammonia only weakly adsorbs with ΔE_{ads} = 1.4 kcal/mol (ST8), but the subsequent reaction exhibits a negligible activation energy of $E^{\ddagger}$ = 0.6 kcal/mol (TS7), which leads to the formation of nitramide (ST13). The latter then decomposes into N_2O and water as was shown in Ref. [29]. Also in the case of the reaction with water, only a rather small barrier of $E^{\ddagger}$ = 1.6 kcal/mol (TS6) was calculated. Similarly, to the reaction with ammonia, the heat of adsorption for water is negligible (ST9), but the formation of nitric acid (ST12) is exothermic. Thus, the $Z^-[NO_2]^+$ can be seen as a rather short-lived intermediate in the NO_2-SCR. Finally, an interchange between the two NO_x^+ species is also possible. Starting from NO_2^+, a reaction with NO only exhibits a barrier of $E^{\ddagger}$ = 1.1 kcal/mol (TS5) to form NO_2 together with $Z^-[NO]^+$ (ST11). Because of the exothermic character of this reaction, this step might only be accessed within the framework of the fast SCR, when both overall reactions, the fast and the NO_2-SCR, interact with each other. Similar to our discussion on nitrous acid reactions, the nitric acid might decompose into water and NO_2^+ in the reverse direction of the described mechanism involving TS6. This would require to overcome a barrier of $E^{\ddagger}$ = 25.3 kcal/mol. Thus, two pathways for the NO_2-SCR can be deduced from this analysis to be of potential importance, depending on either first the formation of sym-N_2O_4 or as-N_2O_4. The formation of the symmetric isomer is followed by a rather high barrier for the decomposition into nitrous acid and the NO_2^+. While nitrous acid decomposes into NO^+ as described in the pathway of the fast SCR, NO_2^+ reacts with ammonia to nitramide. In the case of as-N_2O_4, the initial barrier for the formation is higher than the corresponding formation of the symmetric isomer, but the subsequent decomposition into NO^+ and nitric acid exhibits only a negligible activation energy. The highest barrier in this process is then the decomposition of the nitric acid with a barrier similar in magnitude to the decomposition of sym-N_2O_4. In both cases, the stoichiometry leads to the formation of one nitrosamine and one nitramide, which results in the equimolar formation of nitrogen and N_2O. This is in good agreement with the experimentally observed values [23], at least at low temperatures. A firm conclusion of preferred pathways cannot be drawn from the activation energies. This requires the microkinetic modeling discussed in the next section.

However, a comparison of the presented pathways for the fast and the NO_2-SCR reveals, consistent with the experimental literature [11,22], a higher activity for the fast SCR. Both the formation of the dimerized nitrogen oxide and the decomposition of the resulting acid exhibit a significantly lower barrier for the fast SCR as for the NO_2-SCR.

A comparison of the new pathways with our previous results in the initial formation of NH_2NO_x from a reaction of N_2O_y co-adsorbed on NH_4^+ reveals that the formation of the dimerized nitrogen oxides is slightly lower in both cases (as-N_2O_y) in the absence of ammonia, but within comparable orders of magnitude. However, in the presence of ammonia, as a first step, the ammonium ion is activated by releasing a proton back to the catalytic surface, which exhibits a rather high barrier of ~20 kcal/mol. Thus, it can be concluded that the decomposition of the N_2O_y species on the Brønsted acid is favorable with respect to lower activation energies. However, these steps require the adsorption of NO_2 on a void active site that might be blocked by the strong adsorbing ammonia. This leaves an uncertainty whether the presented pathways are active or blocked due to lack of free active sites.

3.2. Microkinetic modeling

In this section, we compare the results obtained from the microkinetic model with the experimental literature. Reactor simulations were performed in an ideal plug flow reactor with the catalyst being evenly distributed. The number of active sites was calculated based on the mass of the catalyst and its Si/Al ratio, assuming that the number of aluminum atoms is equal to the number of active sites. The thermodynamic database of the gas-phase species in CHEMKIN was obtained either from the database of the Gas Research Institute [75] or created from experimental heats of formations from the literature [76,77] in combination with calculated contributions from translation, rotation, and vibration for the temperature effect. For other gas-phase species, for which no experimental values were available, the heats of formation were calculated from related heats of reaction obtained with the CBS-QB3 method. The values of all gas-phase species are listed in Table 1. For the surface species, the heat of formation can be obtained from the thermodynamic data (Table S4, Supporting information). The reference states for the definition of the heat and the entropy of formation of the surface species and the calculate corrections are listed in Table S1 in the Supporting information. In the column denoted with "extra", the adjustments of the heat of formations within the accuracy of the DFT are stated. The reaction rates of all reversible elementary steps are listed in Table S3 in the Supporting information for the applied direction. All adjustments on the activation energies and pre-exponential factors are stated as "Modifications".

The subsequent discussion is subdivided into the adsorption of ammonia, the NO_2-SCR, the fast SCR, and the oxidation of ammonia.

3.2.1. Adsorption of ammonia

It is well known that ammonia strongly adsorbs on Brønsted acids by forming ammonium ions [78]. While this is assumed to block the oxidation of NO to NO_2 in the standard SCR [79], it similarly might also inhibit the fast and NO_2-SCR, depending on the accessed pathways. Therefore, it is expected that the adsorption of ammonia has a significant impact on the reactivity of the SCR. We considered the adsorption of ammonia in three layers in terms of, first, the formation of the ammonium ion NH_4^+ with a Brønsted acid and, then, the co-adsorption of two further ammonia molecules. Based on the implementation of the kinetics of elementary steps in CHEMKIN, the ammonia adsorption is described as a Langmuir type isotherm (for details of the derivation see the Supporting Information).

$$a_{NH_3}\left[\frac{\text{mmol}}{\text{g}}\right] = \frac{K_1 \cdot p_{NH_3} + 2 \cdot K_1 \cdot K_2 \cdot p_{NH_3}^2 + 3 \cdot K_1 \cdot K_2 \cdot K_3 \cdot p_{NH_3}^3}{1 + K_1 \cdot p_{NH_3} + K_1 \cdot K_2 \cdot p_{NH_3}^2 + K_1 \cdot K_2 \cdot K_3 \cdot p_{NH_3}^3} \cdot \text{Sites}\left[\frac{\text{mmol}}{\text{g}}\right] \tag{11}$$

The corresponding elementary steps are also outlined in Table S3 of the Supporting information in the section "General Adsorption". The ammonium ion is denoted as "NH3(S)", the co-adsorbed state of a second ammonia molecule as "NH3x2(S)" and of a third molecule as "NH3x3(S)". The isotherm reflects the steady state behavior of the microkinetic model for the ammonia adsorption in the absence of any reaction. Because of its potentially strong impact on the SCR, we analyze here whether the enforced mathematical description of the adsorption in CHEMKIN is capable to describe ammonia adsorption experiments.

In Fig. 1, the threefold ammonia co-adsorption is shown on an intersection of the straight and the zig-zag pore of the zeolite, including a framework aluminum. This is in accordance with the experimental literature in which adsorption sites are correlated to the aluminum content [80,81] of the zeolite and a layer-by-layer adsorption is suggested [82–86] as is applied here. The experimental heat of adsorption (144–158 kJ/mol [87,88], 150 kJ/mol [89,90], 145 kJ/mol [81], 128 kJ/mol [85]) is in reasonable agreement with our calculated value (137 kJ/mol) for the ammonium ion formation. Furthermore, Dumesic and coworkers [89] and Gorte and coworkers [81] both found a sharp drop in the heat of adsorption (to 70 kJ/mol and 85 kJ/mol, respectively) with increasing coverage of ammonia on the surface above a certain limit prior to which the heat remains rather constant. Gorte et al. have correlated this limiting coverage to the number of Brønsted acids available in the catalyst and thus with the formed ammonium ions. For the co-adsorption of ammonia to the ammonium ion, we calculated a heat of adsorption of H_{ads} = 100 kJ/mol for the first and H_{ads} = 68 kJ/mol for the second molecule. These values are in good agreement with the experimental value and thus can explain the reduced heat of adsorption at higher coverages. In Fig. 6a and b, the adsorption isotherms from two independent experimental studies [82,90] are compared to our calculated results of Eq. (11). In both sets, reasonable agreement is obtained with only slight modifications in the thermodynamic data. Specifically, we have used a slightly reduced heat of adsorption for the first ammonia (H_{ads} = 127 kJ/mol), in agreement with the value of Bonelli and coworkers [85]. For the co-adsorption of ammonia, the reduction of heat of formations leads to $H_{co\text{-}ads}$ = 95 kJ/mol for the first and $H_{co\text{-}ads}$ = 77 kJ/mol for the second molecule, in reasonable agreement with the experimental data. However, for both isotherm measurements, the Si/Al ratio had to be modified to avoid overestimation of the adsorbed ammonia. For the data of Valyon et al. [82], the ratio was modified from 33.4 to 50 and those of Auroux and coworkers [90] from 18 to 26. Therewith, our results suggest that, regardless of the overall aluminum content in the catalyst, a significant fraction either does not contribute to the surface acidity (e.g., extra framework aluminum) or is not accessible by ammonia. This finding is supported by the fact that Auroux and coworkers [90] found an amount of 720 μmol/g of strong acid sites from calorimetric measurements, which correlates well with the modified Si/Al ratio of 26, which corresponds to 640 μmol/g. Also Brandenberger et al. [26] observed in SCR a 21% reduced Brønsted acidity in their H-ZSM5 sample, as was expected from the Si/Al ratio. While heterogeneity of the active sites cannot be excluded,

Table 1
Heat of formation of gas-phase species.

	$\mathbf{H}_f^0$ (kcal/mol)
NH_3	−10.97[a]
NO	21.56[b]
NO_2	7.91[c]
N_2O	19.60[b]
H_2O	−57.80[a]
HNO	23.80[c]
t-HONO	−18.34[c]
HNO_3	−32.10[c]
NH_2OH	−11.19[d]
NH_2NO	17.79[d]
NH_2NO_2	0.35[d]
as-N_2O_3	19.80[c]
ct-N_2O_3	30.25[d]
sym-N_2O_4	2.19[b]
as-N_2O_4	9.13[d]
c-HNNO	53.66[d]
NH_4NO_2	−38.29[d]
NH_4NO_3	−55.36[d]

[a] See Ref. [75].
[b] See Ref. [76].
[c] See Ref. [77].
[d] Calculated with CBS-QB3.

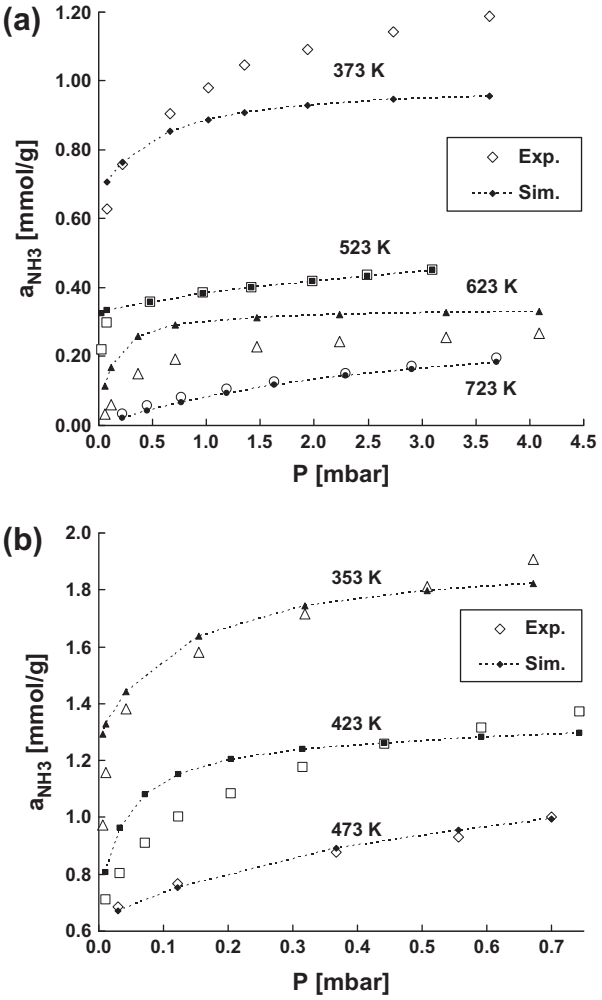

Fig. 6. Comparison of simulated and experimentally measured adsorption isotherms of ammonia on H-ZSM5. Data in (a) corresponds to Ref. [82] and in (b) to Ref. [90].

according to Datka and Gil [91], most experimentalists report a rather homogeneous acidity of H-ZSM5 [81,89,90]. At low temperatures (T = 373 K, Fig. 6a), the calculated isotherm suggests the potential co-adsorption of even a fourth ammonia molecule. However, the isotherms at 473 and 523 K can also be represented by considering only two layers of ammonia per active site and at 623 and 723 K even the ammonium ions are sufficient. Thus, in the SCR, the adsorption in up to two layers is relevant at temperatures above 500 K.

3.2.2. Modeling of the NO_2-SCR

The kinetic modeling of the NO_2-SCR is compared to the results of Stevenson and Vartuli [23] who used a tubular reactor with an inner diameter of 3.49 mm, a volume of the catalytic bed of 0.41 cm^3 and a length of 4.3 cm. At a volumetric flow of 1000 sccm, 0.019 g catalyst with a ratio of Si/Al = 22 was used. The composition of the reactant gas was 500 ppm of both, NO_2 and NH_3, in 1% oxygen and He as balance. Conversions at 300, 350, and 400 °C were reported. Regarding the kinetic parameters of the N_2O_4 formation, comparison of the calculated gas-phase decomposition of the symmetric isomer with experimental data [92] revealed an overestimation of the activation energy by approximately 5 kcal/mol and a low pre-exponential factor. Therefore, in all cases, the activation energy of the formation or decomposition of N_2O_4 was reduced correspondingly, and the pre-exponential factor was increased by one order of magnitude for both isomers. Our model was tuned further based on sensitivity analysis of all reactions and the heat of formations of all surface species, as described by Salciccioli et al. [40]. The sensitive reaction rates and heat of formations (see Tables S1 and S3) were manually adjusted within accuracy to capture approximately the conversion of NO_2 at 350 °C. Fig. 7 shows the conversion of NO_2 and the fraction of active sites occupied by ammonia and the void sites vs. temperature. Very good agreement between the model and the experimental data is observed. Reaction path analysis reveals that the main path entails adsorption of NO_2 on an empty active site followed by the co-adsorption of a second NO_2 and the subsequent formation of as-N_2O_4. The latter decomposes into $Z^-[NO]^+$ and nitric acid, which desorbs to the gas-phase. Ammonia then adsorbs to the nitrosyl ion and forms nitrosamine together with the restoration of the Brønsted acid. The nitric acid adsorbs on a free active site and decomposes into $Z^-[NO_2]^+$ by forming water, which desorbs to the gas-phase. In analogy to the nitrosyl ion, ammonia adsorbs on the $Z^-[NO_2]^+$ and forms nitramide. Nitrosamine and nitramide then decompose into nitrogen and nitrous oxide respectively together with water. Thus, the initial stage of the mechanism, the formation of NH_2NO_x follows the suggested pathways of the preceding Section 3.1 while the decomposition of these intermediates is described in our previous papers [27,29]. A direct reaction of N_2O_4 with the adsorbed ammonium can be neglected over the entire range of temperature. The same is true for bimolecular reactions of nitric acid. The bimolecular reaction of nitric acid with an ammonium ion, as described in Ref. [29] to proceed via adsorbed ammonium nitrate to nitramide, only slightly contributes to the decay of the acid at low temperatures. A slight reduction of the activation energy of the dehydration step and of the heat of formation of the adsorbed ammonium nitrate leads to a significantly higher contribution of this bimolecular reaction to the reduction of nitric acid up to temperatures of 550 K. However, the impact on the overall conversion of NO_2 is negligible. Thus, a significant contribution of this reaction in the NO_2-SCR mechanism cannot be excluded but also not proven with our model. With that, the relevant reactions can be summarized with the sequence of reactions (5), (4), (7), and (8) for the formation of nitrosamine and nitramide via NO^+ and NO_2^+. Furthermore, the decomposition of NH_2NO_x

$$NH_2NO \leftrightarrow N_2 + H_2O \quad (12)$$

$$NH_2NO_2 \leftrightarrow N_2O + H_2O \quad (13)$$

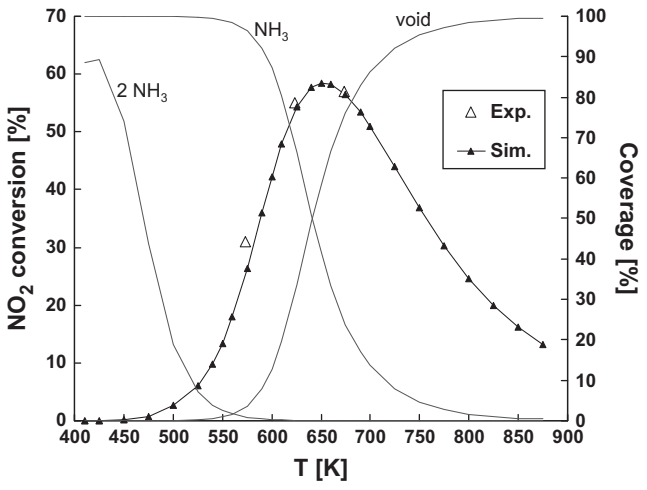

Fig. 7. Simulated conversion of NO_2 vs. temperature in comparison to data from Ref. [23]. On the second axis, the coverages of ammonia and the void sites are shown.

and the reaction of nitric acid with adsorbed ammonia via ammonium nitrate to nitramide and water are potentially relevant.

$$NH_3 + HNO_3 \leftrightarrow NH_4NO_3 \leftrightarrow NH_2NO_2 + H_2O \quad (14)$$

The detailed balances of the elementary steps are outlined in Table S3 in the Supporting information, denoted with "NO_2 SCR, this work", "NH_2NO_x decomposition", and "$NH_3 + HNO_3$". NO^+ is denoted as "NOZ" and NO_2^+ as "ZNO_2". The pathway of reactions (5), (4), (7), and (8) is also highlighted in the schematic of Fig. 4. Furthermore, under our conditions, the oxidation of ammonia was not found to significantly contribute to the conversion. This somewhat contradicts the observed stoichiometry of Stevenson and Vartuli [23] who stated a consumption of about 1.4 mol ammonia per mole NO_2, which they partially attributed to the SCO. In addition, the lack of the ammonia oxidation in our simulation implies a constant ratio of produced nitrogen to nitrous oxide (equal to one). This is in agreement with the reports of Eng and Bartholomew [93] and Busca and coworkers [21], but only at 300 °C for the results of Stevenson and Vartuli (they observed a decay of the N_2O/N_2 ratio at higher temperatures). This could be due to an additional reaction mechanism relevant in the NO_2-SCR at elevated temperatures or to the partial decomposition of NO_2 to NO and oxygen, enforced by thermodynamic equilibrium conditions.

From the sensitivity analysis, it can be concluded that the rate-limiting step is the desorption of nitric acid from $Z^-[NO]^+$ over the entire range of temperature. The dependence of conversion on temperature can be explained based on two main effects. At low temperatures, the reaction is mainly limited by the strong ammonia adsorption as ammonium ion, which blocks the active sites. Thus, the Brønsted acid is not available for the adsorption of NO_2, which is a pre-requisite for the subsequent formation of N_2O_4 and the decomposition to NO^+. This can be seen in Fig. 7 where an obvious correlation of the left shoulder of the conversion with the void fraction of active sites is seen. No other species besides ammonia is present on the surface in significant fraction. The decrease of conversion with elevated temperatures can be traced to the thermodynamic equilibrium of as-N_2O_4. A partial equilibrium analysis (PE) [40] over the whole range of temperatures (Fig. S4, Supporting information) reveals that above 600 K all the steps prior to the rate-limiting nitric acid desorption are in partial equilibrium. The equilibrium surface coverages of the corresponding species vs. temperature show that even though the surface coverage of NO_2 increases up to ~750 K, the concentration of the as-N_2O_4 steadily decreases. Accordingly, the concentration of the subsequent intermediate and the reaction rate of the rate-limiting elementary step decrease with increasing temperature.

3.2.3. Modeling of the fast SCR

For the fast SCR, we compared our model against the data of Schwidder et al. [10] with a tubular reactor of 6 mm inner diameter and an assumed length of 5 cm. The amount of catalyst was 10 mg with a ratio of Si/Al = 14 and a flow rate of Q = 183.3 ml/min. The composition of the reactant gas was 500 ppm NO, 500 ppm NO_2, and 1000 ppm ammonia in 2% oxygen and balance helium. Similarly, as with the NO_2-SCR, comparison of the gas-phase decomposition of as-N_2O_3 into NO and NO_2 from experiments [92] with our simulations revealed an underestimation of the pre-exponential factor by an order of magnitude. Thus, we have accordingly adjusted all N_2O_3 decompositions. Further fine-tuning, as described in Section 3.2.2, was accomplished without further adjustment of the NO_2-SCR parameters. The resulting model is compared against experimental data in Fig. 8a. It can be seen that the simulated and the measured conversion curves vs. temperature agree quite well. Yet, our model slightly underestimates at low temperatures whereas above 725 K, the NO_2 conversion significantly deviates. This deviation supports our discussion on an additional reaction step in the NO_2-SCR capable to convert NO_2 without the production of nitrous oxide. Fig. 8b shows the conversion of ammonia in comparison to the combined conversion of NO and NO_2 and the respective experimental data. While in both cases, the fast and the NO_2-SCR require an equimolar conversion of ammonia and NO_x, the combined NO_x conversion curve reflects the ammonia conversion in the absence of its oxidation. Thus, from the deviation of the two curves, the influence of the SCO can be seen to be rather small, starting at ~600 K. The deviation of the NO_x curve from the experimental data at high temperatures is clearly related to the deviation of the NO_2-SCR described above. It should be noted from Fig. 8b that the experimental NO_x conversion is higher than the ammonia conversion over a wide range of temperature. This reflects also the uncertainty in the experimental data set, because even in the absence of the SCO, this behavior would require the formation of nitrogen without ammonia that is not plausible at these reaction conditions. To check the influence of a potentially reduced amount of accessible Brønsted acids on the combined NO_x conversion, an additional curve is shown in Fig. 8b, corresponding to 80% of the amount of active sites derived from the Si/Al ratio. This analysis is done because the ammonia isotherms (Section 3.2.1) indicate a reduced amount of Brønsted acids compared to the total aluminum present in the catalyst. The value of 80% is related to the experimentally stated value of Brandenberger et al. [26]. It can be seen that the impact of a reduction of active sites of about 20% on the conversion is small.

Reaction path analysis indicates that similarly to the NO_2-SCR pathway, the mechanism proceeds via the adsorption of NO_2 and co-adsorption of NO prior to the formation of N_2O_3. Here, the asymmetric isomer is dominant, though to a certain extent, the path via the cis-trans form is accessed, as well. The decomposition of the dimer leads to $Z^-[NO]^+$ and nitrous acid, which desorbs. The nitrosyl ion reacts then with ammonia to nitrosamine that decomposes to nitrogen and water. The fate of the nitrous acid is dependent on the temperature. While at elevated temperatures, it decomposes on a free active site into the nitrosyl ion and water and at low temperatures, it, at least in part, co-adsorbs to an ammonium ion and reacts via ammonium nitrite to nitrosamine and water. The relevant reactions can be summarized with the sequence of reactions (2)–(4) for the formation of nitrosamine via NO^+ and the decomposition of the latter according to reaction (12). Furthermore, the reaction of nitrous acid with adsorbed ammonia via ammonium nitrite to nitrosamine and water is relevant.

$$NH_3 + HONO \leftrightarrow NH_4NO_2 \leftrightarrow NH_2NO + H_2O \quad (15)$$

The detailed balances of the elementary steps are outlined in Table S3 in the Supporting information, denoted with "fast SCR, this work" and "NH_3 + HONO". NO^+ is denoted as "NOZ". Furthermore, the pathway of reactions (2)–(4) is highlighted in the schematic of Fig. 2. In addition, the NO_2-SCR mechanism, as described in Section 3.2.2, also contributes to a certain extent to the conversion of NO_x, but the pathway via N_2O_3 is dominant. The rate-limiting step with respect to the production of nitrogen was found to change with temperature. At low temperatures up to 550 K, the co-adsorption of NO to NO_2 prior to the formation of N_2O_3 is limiting. At higher temperatures, the desorption of nitrous acid from $Z^-[NO]^+$ limits the overall reaction. Furthermore, in the range between 600 and 750 K, the desorption of nitric acid from the nitrosyl ion becomes important, i.e., an increase in the desorption rate causes a reduction of the nitrogen formation. This is obvious in light of this step being rate-limiting for the competing NO_2-SCR and given the fact that in this temperature range, NO_2 is nearly completely consumed. Thus, an increase of the NO_2-SCR rate would reduce the fast-SCR pathway. The left shoulder of the conversion curve again correlates to the strong adsorption of ammonia, which blocks active sites at low

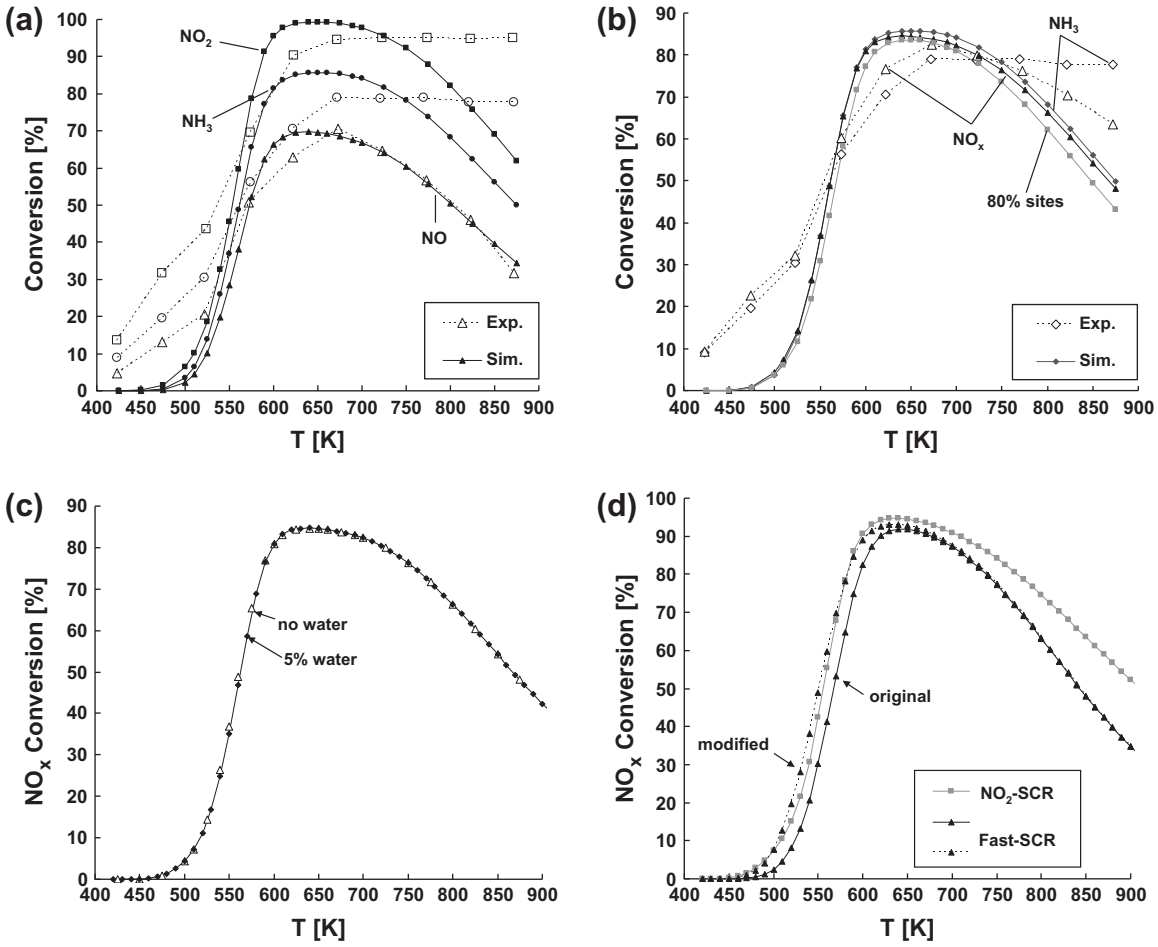

Fig. 8. (a) Simulated conversion of NO, NO_2, and NH_3 vs. temperature in comparison to data from Ref. [10]. (b) Simulated conversion of combined NO_x and NH_3 vs. temperature in comparison to the data of Ref. [10]. (c) Influence of 5% water on the conversion of NO_x. (d) Comparison of the fast and the NO_2 at equivalent conditions.

temperatures. At high temperatures, the decreasing conversion is due to the thermodynamic limitation of the N_2O_3 adsorbed on the surface. Similarly to the NO_2-SCR, Fig. S5 in the Supporting information shows that at temperatures above 650 K, adsorption of NO_2, co-adsorption of NO, and formation of N_2O_3 are in partial equilibrium. The equilibrium concentration of the latter species, however, has a maximum between 600 and 625 K after which it decreases and, thus, causes the decrease in overall conversion.

In Fig. 8c, the influence of 5% water on the conversion of NOx in the fast SCR is shown, and it can be obtained that the impact is negligible. The very slight deviation of the two curves results from an additional blocking of the active site by water.

In Fig. 8d, a comparison between the fast and the NO_2 SCR is shown at equivalent conditions ($NH_3 = NO_x = 1000$ ppm). For the fast SCR, the elementary steps of the NO_2 SCR have been removed from the model to eliminate their superimposing effect on the conversion and thus to illustrate the activity of the actual fast SCR only. Despite the conclusion drawn from the DFT results and the comparison of the energy diagrams of the two pathways that the fast SCR should be more active than the NO_2 SCR, higher conversions are obtained for the latter. However, by increasing the pre-exponential factor of the rate constant of the co-adsorption of NO to adsorbed NO_2, the fast SCR becomes slightly more active than the NO_2 SCR up to the maximum of the conversion curve (dotted line in Fig. 8d). It should be noted that within the adjustment of the NO_2 SCR, the analog rate of the co-adsorption of NO_2 to adsorbed NO_2 was increased as well. Thus, these considerations reflect the qualitative character of our model that only allows for the conclusion that both reactions exhibit a similar activity but not which one is slightly more favorable. For such a conclusion, a refinement of the relevant elementary steps with higher order quantum chemical calculations as well as more experimental data for adjustment and validation of the kinetic parameters would be necessary.

To sum up, from the reaction path analysis for the NO_2 and the fast SCR, it can be concluded that the mechanism, elucidated with our model, combines aspects of several suggestions in the literature for various types of catalysts. The most common sequence of reactions includes the disproportionation of N_2O_4 to nitrite and nitrate and the subsequent reaction of ammonia with these intermediates via ammonium nitrite to nitrogen and via ammonium nitrate to nitrous oxide. The reaction of nitric oxide with a nitrate to nitrite is the key step in the fast SCR. This was suggested by Sachtler et al. [94,95] for Ba-NaY, by Koebel et al. [96,97] for a vanadium-based catalyst and by Tronconi et al. [8], Kröcher and coworkers [6], and Iwasaki and Shinjoh [98] for Fe-ZSM5. Furthermore, from isotopic labeling on Fe-ZSM5, Sachtler and coworkers [99] found that molecular nitrogen is formed from a 1:1 stoichiometry between ammonia and a nitrogen oxide and suggested ammonium nitrite as essential intermediate. In analogy to these suggestions, we obtained the disproportionation of N_2O_3 and N_2O_4, however, not by forming two acids as would be the case for a reaction with water, but only one acid (nitrous and nitric acid, respectively) together with a nitrosyl ion as balancing charge on the zeolite framework. This is only in agreement with the suggestions of Lavalley and coworkers [31]. The NO^+, however, is readily

consumed by ammonia to nitrosamine in accord with Richter et al. [30] rather than reacting with water to nitrous acid. The proposed reaction of nitrous or nitric acid with adsorbed ammonia via ammonium nitrite and nitrate was observed to be relevant at low temperatures, via the additional intermediate formation of nitrosamine for the nitrite, as proposed by Richter et al. [30], and nitramide for the nitrate. At high temperatures, we found the nitrous acid to decompose on a Brønsted acid to nitrosyl, in agreement with Richter et al. and Lavalley et al., and the nitric acid to decompose to NO_2^+ that further reacts with ammonia to nitramide. The suggested reaction of nitric oxide with a nitrate (here nitric acid) was found to not proceed at all. The proposed mechanism by Eng and Bartholomew [93] involves the direct attack of nitrogen oxides on adsorbed ammonium ions. This was found not to proceed in our model, although it has to be mentioned that Eng and Bartholomew considered a complex that involves two adjacent occupied active sites. We only considered the reaction on one single Brønsted acid and, thus, the suggestion of Eng and Bartholomew cannot be excluded. Despite the similarities and deviations of our model with the widely suggested mechanism, as stated above, it further has to be noted that these studies mainly refer to ion-exchanged zeolites, or to vanadium-based catalysts. Deriving an analogy or transferring the mechanism to the H-form catalyst is very speculative if one does not want to claim that it mainly proceeds on the same type of site in all catalysts, e.g. the Brønsted acids.

3.2.4. Oxidation of ammonia

In order to account for the potential influence of the oxidation of ammonia as a side reaction, we have included the SCO reaction mechanism in the discussion on the NO_2-SCR and the fast SCR. Fine-tuning of this submechanism was carried out by comparing to the data of Akah et al. [15]. The volumetric gas flow was set to $Q = 200$ ml/min with a reactant gas composition of 500 ppm ammonia in 2% oxygen and balance helium. Furthermore, 0.1 g catalyst with a ratio of Si/Al = 15 was employed, and we assumed a tubular reactor with 6 mm diameter and 5 cm long as in the modeling of the fast SCR. Fig. 9 shows the conversion of ammonia vs. temperature. Reasonable agreement between simulation and experiment is found. The mechanism consists of three parts as described in detail in Ref. [28]. First, oxygen reacts with adsorbed ammonia forming nitroxyl and water. Then, HNO reacts in an intramolecular reaction to NO and adsorbed H_2NO, which after reaction with another nitroxyl molecule leads to hydroxylamine and a second nitrogen oxide. The NH_2OH finally reacts with a third HNO to nitrosamine, which decomposes into nitrogen and water.

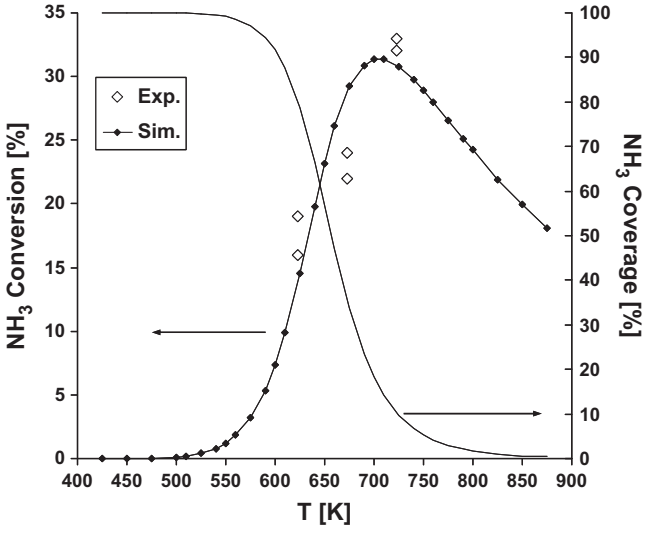

Fig. 9. Simulated conversion of NH_3 from reaction with oxygen in comparison to data from Ref. [15].

$$NH_3 + O_2 \leftrightarrow HNO + H_2O \quad (16)$$

$$HNO + HNO \leftrightarrow H_2NO + NO \quad (17)$$

$$H_2NO + HNO \leftrightarrow NH_2OH + NO \quad (18)$$

$$NH_2OH + HNO \leftrightarrow NH_2NO + H_2O \quad (19)$$

The detailed steps of reactions (16)–(19) are presented in Table S3 in the Supporting information, denoted with "$NH_3 + O_2$", "HNO + HNO", "HNOH + HNO", and "NH_2OH + HNO". However, this pathway leads to a deviation in the selectivity of the reaction with respect to nitrogen compared to experiments. While experiments suggest selectivity to nitrogen of about 65%, our model predicts only 50%. Even though we have included potential reactions of nitroxyl with NO, none of them was found to be significant at these conditions to account for this deviation. Thus, the most reasonable explanation is oxidation of part of NO to NO_2 followed by the fast SCR mechanism. Our proposed mechanism for this oxidation [27] is however only capable of accounting for the low temperature conversion (compare Halasz et al. [79]), but not for the high temperature regime. Nevertheless, the rate-limiting step, the reaction of oxygen with an adsorbed ammonium ion to adsorbed NH_3OOH^+, was found to be independent of temperature. Thus, the rates of the subsequent steps producing NO and N_2 from the decay of nitroxyl do not significantly influence the overall reaction rate of the SCO, and thus, oxidation of a fraction of NO to NO_2 is not expected to significantly change the conversion vs. temperature. Furthermore, in the NO_2-SCR, the oxidation of NO is less relevant because the produced NO directly reacts with NO_2 according to the fast-SCR mechanism. Therefore, it can be concluded that the impact of the ammonia oxidation on the fast and the NO_2-SCR is only minor and is not expected to account for the observed deviation of the NO_2-SCR at high temperatures.

In contrast to the SCR reactions, the ammonium ion does not block the active sites but actively participates in the reaction. The maximum of the conversion at ~700 K is related to the decreasing amount of ammonia adsorbed on the catalyst. The left shoulder of the curve is related to the rate-limiting initial reaction of oxygen with the adsorbed ammonium ions.

4. Conclusions

The mechanisms of the three major sets of the selective catalytic reduction of nitrogen oxides, namely the NO_2-SCR, the fast SCR, and the SCO, were analyzed using microkinetic modeling. In a first part, additional pathways including the intermediate formation of $Z^-[NO_x]^+$ species, calculated with DFT, were presented and compared to prior calculated mechanisms that involve the reaction of NO_x with adsorbed ammonium ions. It was concluded that, based on activation energies, the reported new sequence of reactions is more probable to be responsible for the activity of the H-ZSM5 in the fast and the NO_2-SCR though an uncertainty remains with respect to the potential blocking of active sites by ammonia. The microkinetic model, which includes the DFT-calculated reaction mechanisms of our previous works [27–29] and of Section 3.1, showed reasonable agreement with different sets of experimental data. First of all, the crucial adsorption of ammonia on Brønsted acids indicates co-adsorption of up to four ammonia molecules on an active site at low temperatures. In addition, our model suggests that only a fraction of the framework aluminum is capa-

ble to bind ammonia as ammonium ion. This might be explained by a potential inaccessibility of a certain fraction of Brønsted acids within the microstructure of the zeolite. For the NO_2-SCR, the reaction was found to proceed in the following sequence. First, NO_2 adsorbs and a second NO_2 co-adsorbs prior to the formation of as-N_2O_4 that then decomposes into nitric acid. The latter then desorbs and leaves a nitrosyl ion on the catalyst that subsequently reacts with ammonia to nitrosamine. The nitric acid decomposes on an active site into water and $Z^-[NO_2]^+$ that reacts with ammonia to nitramide. Finally, nitramide and nitrosamine decompose into water and nitrous oxide and nitrogen, respectively. Furthermore, at low temperatures, nitric acid potentially reacts directly with an ammonium ion to nitramide and water. The rate-limiting step is the desorption of nitric acid, leaving the nitrosyl ion on the zeolite. The observed maximum in the conversion vs. temperature was related to the blocking of sites by ammonia at low temperatures and to the thermodynamic equilibrium conditions of the intermediate as-N_2O_4 at elevated temperatures. For the mechanism of the fast SCR, in analogy to the NO_2-SCR, it was concluded that as-N_2O_3 is formed as intermediate on the active site, which then decomposes into nitrous acid together with the formation of a nitrosyl ion. Here, the decomposition of the acid leads to a second nitrosyl ion or, at low temperatures, the acid directly reacts with an ammonium ion to nitrosamine and water. In addition, the superposition of the NO_2-SCR causes deviation in NO and NO_2 conversion. At high temperatures, the desorption of nitrous acid from the nitrosyl ion is rate-limiting in analogy to the NO_2-SCR mechanism while, at low temperatures, the co-adsorption of NO to NO_2 prior to the formation of the intermediate as-N_2O_3 is rate-limiting. The observed maximum can be related to the blocking of the active sites by ammonia at low temperatures and to the thermodynamic equilibrium of as-N_2O_3 at high temperatures. Finally, the governing pathway of the SCO entails the reaction of oxygen with an ammonium ion to nitroxyl and water and subsequently a self-reaction of HNO, which releases NO to the gas-phase and leaves H_2NO on the active site. The latter reacts with another HNO to hydroxylamine followed by the reaction with a third nitroxyl to nitrosamine and water. The limiting factors in this reaction were found to be the initial elementary step between the ammonium ion and oxygen and at high temperatures the thermodynamic limitation of adsorbed ammonia on the active site. The deviation between calculated and experimentally observed selectivity toward nitrogen in the SCO is attributed to oxidation of part of the produced NO to NO_2 followed by the fast SCR mechanism. However, at the present conditions for the SCR, the ammonia oxidation was found to have only a minor impact. Thus, the deviation of the calculated NO_2-SCR at high temperatures (above 725 K) may be due to an additional reaction mechanism or result from the decomposition of NO_2 to NO and oxygen followed by the accession of the fast SCR.

In summary, based on first principles' microkinetic modeling, we have elucidated the reaction mechanism of the fast and the NO_2 SCR on H-ZSM5 with Brønsted acids as active sites. The results are to a large extent in agreement with experimental data, and although our model is rather qualitative, several conclusions were drawn beyond experimental findings. Furthermore, high activities of ion-exchanged and H-form zeolites are observed for the fast SCR at equivalent reaction conditions. Considering the fact that metal-exchanged zeolites usually contain significant amounts of Brønsted acids, superposition of contributions of the two different active sites and coupling in terms of intermediate species or a direct interaction seems reasonable. Assuming a transferability of the H-ZSM5 reaction mechanism to other H-form zeolites, our results might provide new insights and concepts for overall reaction mechanisms of a large group of zeolite-based catalysts.

Acknowledgment

The computations were partly carried out at the Norddeutscher Verbund für Hoch- und Höchstleistungsrechnen (HLRN). The work of DGV was supported by the Department of Energy (DOE) under grant number DE-FG02-05ER25702.

Appendix A

Here, we show the derivation of the effective Hessian as was proposed by Harvey et al. [66,67] based on the work of Koga and Morokuma [68]. In addition, we show the corresponding derivation for the algorithm applied in this work for finding minimum energy crossing points.

Basis is the Lagrangian equation L for the determination of the MECP

$$L(\mathbf{R},\lambda) = E_1(\mathbf{R}) - \lambda\cdot(E_1(\mathbf{R}) - E_2(\mathbf{R})) \tag{A1}$$

by minimizing the energy E_1 on one PES with the constraint that the energies are identical on both PESs at the coordinates $\mathbf{R}^*$ of the MECP. The PESs only differ in the assigned spin state. At the MECP the energy E_1 and the Lagrangian L are equal and with that their respective Taylor expansions in the vicinity of this point with a displacement ΔS along the hyperline of the crossing of the PESs (seam). The seam can be defined as the 3N-7 dimensional subspace of both PESs with the vector

$$\mathbf{x} = \nabla E_1(\mathbf{R}) - \nabla E_2(\mathbf{R}) = \mathbf{g}_1 - \mathbf{g}_2 \tag{A2}$$

being orthogonal to the seam at the MECP.

The derivatives of the Lagrangian with respect to the coordinates $\mathbf{R}$ are

$$\frac{\partial L(\mathbf{R},\lambda)}{\partial \mathbf{R}} = \nabla_{\mathbf{R}} L(\mathbf{R},\lambda) = \mathbf{g}_1 - \lambda\cdot(\mathbf{g}_1 - \mathbf{g}_2) = 0|_{\mathbf{R}=\mathbf{R}^*} \tag{A3}$$

$$\begin{aligned}\frac{\partial^2 L(\mathbf{R},\lambda)}{\partial \mathbf{R}^2} &= \nabla^2_{\mathbf{R}} L(\mathbf{R},\lambda) = \nabla^2_{\mathbf{R}} E_1 - \lambda\cdot(\nabla^2_{\mathbf{R}} E_1 - \nabla^2_{\mathbf{R}} E_2)\\ &= \nabla^2_{\mathbf{R}} E_1\cdot(1-\lambda) + \nabla^2_{\mathbf{R}} E_2\cdot\lambda\end{aligned} \tag{A4}$$

With these expressions the Taylor expansion of the energy E at the MECP can be written as

$$\begin{aligned}E_1(\mathbf{R}^* + \Delta\mathbf{S}) =& L(\mathbf{R}^* + \Delta\mathbf{S},\lambda^*) = L(\mathbf{R}^*,\lambda^*) + \Delta\mathbf{S}^T\cdot\nabla_{\mathbf{R}} L(\mathbf{R}^*,\lambda^*)\\ &+ \frac{1}{2}\cdot\Delta\mathbf{S}^T\cdot\nabla^2_{\mathbf{R}} L(\mathbf{R}^*,\lambda^*)\cdot\Delta\mathbf{S} = E_1(\mathbf{R}^*,\lambda^*) + \frac{1}{2}\cdot\Delta\mathbf{S}^T\\ &\cdot\nabla^2_{\mathbf{R}} L(\mathbf{R}^*,\lambda^*)\cdot\Delta\mathbf{S}\end{aligned} \tag{A5}$$

by noticing that the first derivative of the Lagrangian at the coordinates of the MECP is zero as a requirement of the definition of this point to be a minimum on the hyperline of the crossing PESs. Thus, in the Taylor expansion of the energy E_i on either of the two PESs the second derivative of the energy, and with that the Hessian, can be expressed in terms of the second derivative of the Lagrangian which combines contributions from both PESs according to (A4). Finally, only the Lagrange multiplier needs to be determined. It is directly obtained if the corresponding search algorithm for finding of the MECP is applied. However, it can also be calculated independently of the algorithm from Eq. (A3). λ cannot be obtained directly from this equation, but only its absolute value by making use of the norm of the two gradients.

$$\begin{aligned}&\mathbf{g}_1(\mathbf{R}^*) = \lambda^*\cdot(\mathbf{g}_1(\mathbf{R}^*) - \mathbf{g}_2(\mathbf{R}^*))\\ &|\mathbf{g}_1(\mathbf{R}^*)| = |\lambda^*|\cdot|(\mathbf{g}_1(\mathbf{R}^*) - \mathbf{g}_2(\mathbf{R}^*))|\\ &|\lambda^*| = \frac{|\mathbf{g}_1(\mathbf{R}^*)|}{|\mathbf{g}_1(\mathbf{R}^*) - \mathbf{g}_2(\mathbf{R}^*)|} = \frac{|\mathbf{g}_1|}{|\mathbf{x}|}\end{aligned} \tag{A6}$$

In analogy, the separation of the two gradients prior to applying the norm yields in combination with (A6)

$$|1-\lambda^*| = \frac{|\mathbf{g}_2(\mathbf{R}^*)|}{|\mathbf{g}_1(\mathbf{R}^*) - \mathbf{g}_2(\mathbf{R}^*)|} = \frac{|\mathbf{g}_2|}{|\mathbf{x}|} \tag{A7}$$

The reintroduction of the Lagrange multiplier in Eq. (A3) allows for the determination of its correct sign. Inserting the two expressions (A6) and (A7) in (A4) results in the expression of the effective Hessian (10). However, from a practical point of view it is straight forward to only calculate the value of the Lagrange multiplier together with its sign and then directly apply it in (A4) rather than calculating the absolute value of $(1-\lambda)$, as well. In the latter case, this would also require the distinction of cases in order to obtain the correct sign for the difference.

In this work we applied an algorithm with the governing equation for the Lagrangian

$$L(\mathbf{R},\lambda) = E_1(\mathbf{R}) + E_2(\mathbf{R}) - \lambda\cdot(E_1(\mathbf{R}) - E_2(\mathbf{R})) \tag{A8}$$

which minimizes the sum of the energies of the two PESs with the constraint that the energies are equal at the coordinates of the MECP. This results in the corresponding derivatives

$$\frac{\partial L(\mathbf{R},\lambda)}{\partial \mathbf{R}} = \nabla_{\mathbf{R}} L(\mathbf{R},\lambda) = \mathbf{g}_1 + \mathbf{g}_2 - \lambda\cdot(\mathbf{g}_1 - \mathbf{g}_2) = 0|_{\mathbf{R}=\mathbf{R}^*} \tag{A9}$$

$$\begin{aligned}\frac{\partial^2 L(\mathbf{R},\lambda)}{\partial \mathbf{R}^2} &= \nabla^2_{\mathbf{R}} L(\mathbf{R},\lambda) = \nabla^2_{\mathbf{R}} E_1 + \nabla^2_{\mathbf{R}} E_2 - \lambda\cdot(\nabla^2_{\mathbf{R}} E_1 - \nabla^2_{\mathbf{R}} E_2)\\ &= \nabla^2_{\mathbf{R}} E_1\cdot(1-\lambda) + \nabla^2_{\mathbf{R}} E_2\cdot(1+\lambda)\end{aligned} \tag{A10}$$

For the Taylor expansion, it has to be kept in mind that the Lagrangian minimizes the sum of the energies of the two PESs.

$$\begin{aligned}E(\mathbf{R}^* + \Delta\mathbf{S}) =& \frac{1}{2} L(\mathbf{R}^* + \Delta\mathbf{S}, \lambda^*) = \frac{1}{2}\cdot\{L(\mathbf{R}^*,\lambda^*) + \Delta\mathbf{S}^T\cdot\nabla_{\mathbf{R}} L(\mathbf{R}^*,\lambda^*)\\ &+ \frac{1}{2}\cdot\Delta\mathbf{S}^T\cdot\nabla^2_{\mathbf{R}} L(\mathbf{R}^*,\lambda^*)\cdot\Delta\mathbf{S}\} = E(\mathbf{R}^*,\lambda^*) + \frac{1}{4}\cdot\Delta\mathbf{S}^T\\ &\cdot\nabla^2_{\mathbf{R}} L(\mathbf{R}^*,\lambda^*)\cdot\Delta\mathbf{S}\end{aligned} \tag{A11}$$

For the Lagrange multiplier one obtains the absolute value

$$|\lambda^*| = \frac{|\mathbf{g}_1(\mathbf{R}^*) + \mathbf{g}_2(\mathbf{R}^*)|}{|\mathbf{g}_1(\mathbf{R}^*) - \mathbf{g}_2(\mathbf{R}^*)|} \tag{A12}$$

and with that for the effective Hessian of the MECP

$$\mathbf{H}_{eff} = \frac{1}{2}\left\{\nabla^2_{\mathbf{R}} E_1\cdot\left(1 - \left[\pm\frac{|\mathbf{g}_1+\mathbf{g}_2|}{|\mathbf{g}_1-\mathbf{g}_2|}\right]\right) + \nabla^2_{\mathbf{R}} E_2\cdot\left(1 + \left[\pm\frac{|\mathbf{g}_1+\mathbf{g}_2|}{|\mathbf{g}_1-\mathbf{g}_2|}\right]\right)\right\} \tag{A13}$$

Both expressions, Eqs. (10) and (A13) yield the same result in the frequency analysis of the MECP. Though the equation of Harvey et al. is simpler at first, depending on the applied algorithm, it might make sense to derive an alternative expression as shown here and to use the optimized Lagrange multiplier from the MECP search algorithm. Furthermore, this approach allows for the validation of the Lagrange multiplier or the application of a corresponding equation like (A6), and (A12) to obtain a better start value in the search algorithm.

It should be pointed out that the gradients and second derivatives are used in mass weighted coordinates.

Appendix B. Supplementary data

Supplementary data associated with this article can be found, in the online version, at doi:10.1016/j.jcat.2011.08.009.

References

[1] S. Roy, A. Baiker, Chem. Rev. 109 (2009) 4054.
[2] S. Roy, M.S. Hegde, G. Madras, Appl. Energy 86 (2009) 2283.
[3] G. Busca, L. Lietti, G. Ramis, F. Berti, Appl. Catal. B 18 (1998) 1.
[4] Z.M. Liu, S.I. Woo, Catal. Rev. -Sci. Eng. 48 (2003) 43.
[5] Y. Hu, K. Griffiths, P.R. Norton, Surf. Sci. 603 (2009) 1740.
[6] S. Brandenberger, O. Kroecher, A. Tissler, R. Althoff, Catal. Rev. -Sci. Eng. 50 (2008) 492.
[7] M. Devadas, O. Kröcher, M. Elsener, A. Wokaun, N. Soger, M. Pfeifer, Y. Demel, L.M. Mussmann, Appl. Catal. B 67 (2006) 187.
[8] A. Grossale, I. Nova, E. Tronconi, D. Chatterjee, M. Weibel, J. Catal. 256 (2008) 312.
[9] A. Grossale, I. Nova, E. Tronconi, J. Catal. 265 (2009) 141.
[10] M. Schwidder et al., J. Catal. 259 (2008) 96.
[11] R.Q. Long, R.T. Yang, J. Catal. 207 (2002) 224.
[12] A. Grossale, I. Nova, E. Tronconi, Catal. Lett. 130 (2009) 525.
[13] T. Curtin, S. Lenihan, Chem. Commun. (2003) 1280.
[14] A. Akah, C. Cundy, A. Garforth, Appl. Catal. B 59 (2005) 221.
[15] A.C. Akah, G. Nkeng, A.A. Garforth, Appl. Catal. B 74 (2007) 34.
[16] N.N. Sazonova, A.V. Simakov, T.A. Nikoro, G.B. Barannik, V.F. Lyakhova, V.L. Zheivot, Z.R. Ismagilov, H. Veringa, Ract. Kin. Catal. Lett. 57 (1996) 71.
[17] H.M. Kusar, A.G. Ersson, M. Vosecky, S.G. Jaras, Appl. Catal. B 58 (2005) 25.
[18] L. Gang, J. van Grondelle, B.G. Anderson, R.A. van Santen, J. Catal. 186 (1999) 100.
[19] G.S. Qi, J.E. Gatt, R.T. Yang, J. Catal. 226 (2004) 120.
[20] G.S. Qi, R.T. Yang, Appl. Catal. A 287 (2005) 25. 2005.
[21] V. Sanchez-Escribano, T. Montanari, G. Busca, Appl. Catal. B 58 (2005) 19.
[22] M. Wallin, C.J. Karlsson, M. Skoglundh, A. Palmqvist, J. Catal. 218 (2003) 354.
[23] S.A. Stevenson, J.C. Vartuli, J. Catal. 208 (2002) 100.
[24] R.Q. Long, R.T. Yang, Chem. Commun. (2000) 1651.
[25] M. Schwidder, M.S. Kumar, U. Bentrup, J. Perez-Ramirez, A. Brueckner, W. Gruenert, Micropor. Mesopor. Mater. 111 (2008) 124.
[26] S. Brandenberger, O. Kroecher, A. Wokaun, A. Tissler, R. Althoff, J. Catal. 268 (2009) 297.
[27] T.C. Brueggemann, F.J. Keil, J. Phys. Chem. C 112 (2008) 17378.
[28] T.C. Brueggemann, F.J. Keil, J. Phys. Chem. C 113 (2009) 13860.
[29] T.C. Brueggemann, M.-D. Przybylski, S.P. Balaji, F.J. Keil, J. Phys. Chem. C 114 (2010) 6567.
[30] M. Richter, R. Eckelt, B. Parlitz, R. Fricke, Appl. Catal. B 15 (1998) 129.
[31] K. Hadjiivanov, J. Saussey, J.L. Freysz, J.C. Lavalley, Cata. Lett. 52 (1998) 103.
[32] B. Pommier, P. Gelin, Phys. Chem. Chem. Phys. 3 (2001) 1138.
[33] J. Szanyi, J.H. Kwak, R.A. Moline, C.H. Peden, Phys. Chem. Chem. Phys. 5 (2003) 4045.
[34] I. Perdana, D. Creaser, O. Ohrman, J. Hedlund, Appl. Catal. B 72 (2007) 82.
[35] L.J. Broadbelt, R.Q. Snurr, Appl. Catal. A 200 (2000) 23.
[36] A.B. Mhadeshwar, H. Wang, D.G. Vlachos, J. Phys. Chem. B 107 (2003) 12721.
[37] A.B. Mhadeshwar, D.G. Vlachos, J. Phys. Chem. B 109 (2005) 16819.
[38] N. Hansen, A. Heyden, A.T. Bell, F.J. Keil, J. Phys. Chem. C 111 (2007) 2092.
[39] A.A. Gokhale, S. Kandoi, J.P. Greeley, M. Mavrikakis, J.A. Dumesic, Chem. Eng. Sci. 59 (2004) 4679.
[40] M. Salciccioli, Y. Chen, D.G. Vlachos, Ind. Eng. Chem. Res 50 (2011) 28.
[41] D.H. Olson, G.T. Koktailo, S.L. Lawton, W.M. Meier, J. Phys. Chem. B 85 (1981) 2238.
[42] D.H. Olson, N. Khosrovani, A.W. Peters, B.H. Tobym, J. Phys. Chem. B 104 (2000) 4844.
[43] J.G. Fripiata, F. Berger-Andréa, J.-M. André, E.G. Derouanc, Zeolites 3 (1983) 306.
[44] E.G. Derouanea, J.G. Fripiata, Zeolites 5 (1985) 165.
[45] S.R. Lonsinger, A.K. Chakraborty, D.N. Theodorou, A.T. Bell, Catal. Lett. 11 (1991) 209.
[46] A. Chatterjee, A.K. Chandra, J. Molec. Catal. A 119 (1996) 51.
[47] R. Ahlrichs, M. Bär, M. Häser, H. Horn, C. Kölmel, Chem. Phys. Lett. 162 (1998) 165.
[48] A.D. Becke, Phys. Rev. A 38 (1988) 3098.
[49] C. Lee, W. Yang, R.G. Parr, Phys. Rev. B 37 (1988) 785.
[50] A. Schäfer, C. Huber, R. Ahlrichs, J. Chem. Phys. 100 (1994) 5829.
[51] O. Treutler, R. Ahlrichsm, J. Chem. Phys. 102 (1995) 356.
[52] Gaussian 03, Revision C.02, M.J. Frisch, G.W. Trucks, H.B. Schlegel, G.E. Scuseria, M.A. Robb, J.R. Cheeseman, J.A. Montgomery, Jr., T. Vreven, K.N. Kudin, J.C. Burant, J.M. Millam, S.S. Iyengar, J. Tomasi, V. Barone, B. Mennucci, M. Cossi, G. Scalmani, N. Rega, G.A. Petersson, H. Nakatsuji, M. Hada, M. Ehara, K. Toyota, R. Fukuda, J. Hasegawa, M. Ishida, T. Nakajima, Y. Honda, O. Kitao, H. Nakai, M. Klene, X. Li, J.E. Knox, H.P. Hratchian, J.B. Cross, V. Bakken, C. Adamo, J. Jaramillo, R. Gomperts, R.E. Stratmann, O. Yazyev, A.J. Austin, R. Cammi, C. Pomelli, J.W. Ochterski, P.Y. Ayala, K. Morokuma, G.A. Voth, P. Salvador, J.J. Dannenberg, V.G. Zakrzewski, S. Dapprich, A.D. Daniels, M.C. Strain, O. Farkas, D.K. Malick, A.D. Rabuck, K. Raghavachari, J.B. Foresman, J.V. Ortiz, Q. Cui, A.G. Baboul, S. Clifford, J. Cioslowski, B.B. Stefanov, G. Liu, A. Liashenko, P. Piskorz, I. Komaromi, R.L. Martin, D.J. Fox, T. Keith, M.A. Al-Laham, C.Y. Peng, A. Nanayakkara, M. Challacombe, P.M.W. Gill, B. Johnson, W. Chen, M.W. Wong, C. Gonzalez, J.A. Pople, Gaussian, Inc., Wallingford CT, 2004.
[53] B. Peters, A. Heyden, A.T. Bell, A.J. Chakraborty, J. Chem. Phys. 120 (2004) 7877.
[54] A. Heyden, A.T. Bell, F.J. Keil, J. Chem. Phys. 123 (2005) 224101.
[55] J. Baker, J. Comp. Chem. 7 (1986) 385.
[56] A. Heyden, A.T. Bell, F.J. Keil, J. Phys. Chem. B 109 (2005) 1857.
[57] R.J. Kee, F.M. Rupley, J.A. Miller, Chemkin-II: A FORTRAN Chemical Kinetics Package for the Analysis of Gas Phase Chemical Kinetics, Livermore, CA: Sandia National Laboratories Report, SAND89-8009, 1991.
[58] M.E. Coltrin, R.J. Kee, F.M. Rupley, Surface Chemkin: A FORTRAN Package for Analyzing Heterogeneous Chemical Kinetics at a Solid-Surface – Gas Phase Interface, Livermore, CA: Sandia National Laboratories Report, SAND90-8003B, 1991.

[59] D.A. McQuarrie, J.D. Simon, Physical Chemistry, A Molecular Approach, University Science Books, 1997.
[60] C.J. Cramer, Essentials of Computational Chemistry, 2nd ed., John Wiley & sons, 2004.
[61] K.J. Laidler, Chemical Kinetics, third ed., Harper & Row Publisher, New York, 1987.
[62] I. Chorkendorff, J.W. Niemantsverdriet, Concepts of Modern Catalysis and Kinetics, second ed., WILEY-VCH, Weinheim, 2007.
[63] P. Spitzer, C. Zierhofer, E. Hochmair, Biomed. Eng. 5 (2006) 13.
[64] Q. Cui, K. Morokuma, J.M. Bowman, S.J. Klippenstein, J. Chem. Phys. 110 (1999) 9469.
[65] J.N. Harvey, Phys. Chem. Chem. Phys. 9 (2007) 331.
[66] J.N. Harvey, M. Aschi, Phys. Chem. Chem. Phys. 1 (1999) 5555.
[67] J.N. Harvey, M. Aschi, H. Schwarz, W. Koch, Theor. Chem. Acc. 99 (1998) 95.
[68] N. Koga, K. Morokuma, Chem. Phys. Lett. 119 (1985) 371.
[69] M. Page, J.W. Mclver, J. Chem. Phys. 88 (1988) 922.
[70] A.E. Stearn, H. Eyring, J. Chem. Phys. 3 (1935) 778.
[71] F.S. Sousa, P.A. Fernandes, M.J. Ramos, J. Phys. Chem. A 111 (2007) 10439.
[72] N. Hansen, T. Kerber, J. Sauer, A.T. Bell, F.J. Keil, J Am. Chem. Soc. 132 (2010) 11525.
[73] S. Grimme, J. Comput. Chem. 27 (2006) 1787.
[74] B.A. de Moor, M.-F. Reyniers, G.B. Marin, Phys. Chem. Chem. Phys. 11 (2009) 2939.
[75] M. Frenklach, H. Wang, M. Goldenberg, G.P. Smith, D.M. Golden, C.T. Bowman, R.K. Hanson, W.C. Gardiner, V. Lissianski, GRI-MechsAn Optimized Detailed Chemical Reaction Mechanism for Methane Combustion. <http://www.me.berkeley.edu/gri_mech/> (accessed 01.02.09).
[76] B.E. Poling, J.P. O'Connell, J.M. Prausnitz, The Properties of Gases and Liquids, fifth ed., McGraw-Hill, New York, NY, 2001.
[77] M.W. Chase, NIST-JANAF themochemical tables, J. Phys. Chem. Ref. Data 9 (1998) 1. fourth ed..
[78] E.H. Teunissen, R.A. van Santen, A.P.J. Jansen, F.B. van Duijneveldt, J. Phys. Chem. 97 (1993) 203.
[79] I. Halasz, A. Brenner, K.Y. Simon, Catal. Lett. 34 (1995) 151.
[80] L. Shirazi, E. Jamshidi, M.R. Ghasemi, Cryst. Res. Technol. 43 (2008) 1300.
[81] D.J. Parillo, R.J. Gorte, W.E. Farneth, J. Am. Chem. Soc. 115 (1993) 12441.
[82] J. Valyon, G. Onyestyak, L.V.C. Rees, J. Phys. Chem. B 102 (1998) 8994.
[83] F. Lonyi, J. Valyon, Thermochim. Acta 373 (2001) 53.
[84] F. Lonyi, J. Valyon, Micropor. Mesopor. Mater. 47 (2001) 293.
[85] M. Armandi, B. Bonelli, I. Bottero, C.O. Arean, E. Garrone, J. Phys. Chem. C 114 (2010) 6658.
[86] B. Bonelli, M. Armandi, C.O. Arean, E. Garrone, Chem. Phys. Chem. 11 (2010) 3255.
[87] B. Hunger, J. Hoffmann, Thermochim. Acta 106 (1986) 133.
[88] B. Hunger, J. Hoffmann, O. Heitzsch, M. Hunger, J. Therm. Anal. 36 (1990) 1379.
[89] S.B. Sharma, B.L. Meyers, D.T. Chen, J. Miller, J.A. Dumesic, Appl. Catal. A 102 (1993) 253.
[90] B. Dragoi, A. Gervasini, E. Dumitriu, A. Auroux, Thermochim. Acta 420 (2004) 127.
[91] J. Datka, B. Gil, J. Mol. Struct. 596 (2001) 41.
[92] R. Atkinson, D.L. Baulch, R.A. Cox, J.N. Crowley, R.F. Hampson, R.G. Hynes, M.E. Jenkin, M.J. Rossi, J.R. Troe, Atmos. Chem. Phys. 4 (2004) 1461.
[93] J. Eng, C.H. Bartholomew, J. Catal. 171 (1997) 27.
[94] Y. Yeom, J. Henao, M. Li, W. Sachtler, E. Weitz, J. Catal. 231 (2005) 181.
[95] A. Savara, W.M. Sachtler, E. Weitz, Appl. Catal. B 90 (2009) 120.
[96] M. Koebel, M. Elsener, G. Madia, Ind. Eng. Chem. Res. 40 (2001) 52.
[97] M. Koebel, G. Madia, M. Elsener, Selective catalytic reduction of NO and NO2 at low temperatures, Catal. Today 73 (2002) 239.
[98] M. Iwasaki, H. Shinjoh, Appl. Catal. A 390 (2010) 71.
[99] Q. Sun, Z.-X. Gao, H.-Y. Chen, W.M.H. Sachtler, J. Catal. 201 (2001) 88.